Separation Science and Technology
Publication details, including instructions for authors and subscription information:
http://www.informaworld.com/smpp/title~content=t713708471

Comparison of Different Modeling Strategies for Simulation of Carbon Dioxide Absorption in a Coaxial Impinging Streams Absorber

Amir Hossein Harandizadeh[a]; Amir Rahimi[a]; Mohammad Reza Ehsani[b]
[a] Department of Chemical Engineering, College of Engineering, University of Isfahan, Isfahan, Iran [b] College of Chemical Engineering, Isfahan University of Technology, Isfahan, Iran

Online publication date: 20 December 2010

To cite this Article Harandizadeh, Amir Hossein , Rahimi, Amir and Ehsani, Mohammad Reza(2011) 'Comparison of Different Modeling Strategies for Simulation of Carbon Dioxide Absorption in a Coaxial Impinging Streams Absorber', Separation Science and Technology, 46: 1, 105 — 118
To link to this Article: DOI: 10.1080/01496395.2010.492047
URL: http://dx.doi.org/10.1080/01496395.2010.492047

Separation Science and Technology, 46: 105–118, 2011

ISSN: 0149-6395 print/1520-5754 online
DOI: 10.1080/01496395.2010.492047

Taylor & Francis
Taylor & Francis Group

Comparison of Different Modeling Strategies for Simulation of Carbon Dioxide Absorption in a Coaxial Impinging Streams Absorber

Amir Hossein Harandizadeh,[1] Amir Rahimi,[1] and Mohammad Reza Ehsani[2]
[1]*Department of Chemical Engineering, College of Engineering, University of Isfahan, Isfahan, Iran*
[2]*College of Chemical Engineering, Isfahan University of Technology, Isfahan, Iran*

This study presents mathematical modeling of non-isothermal gas absorption in a coaxial two impinging streams absorber (TISA). The governing equations on the performance of these ideal systems for three different models including the plug flow model, the tanks-in-series model, and Markov-Chain analysis are used to model the real system behavior. In order to approach a realistic model, the size distribution of the liquid droplets also is implemented in the models. The comparison between the results of the models with corresponding reported experimental data shows the desirable accuracy of the suggested models. Also, the effects of some operational variables on the average absorption rate and final removal efficiency of TISA are investigated. Results show that for similar operating conditions the removal efficiency of impinging streams absorber is higher than the conventional systems.

Keywords absorption; impinging streams; Markov-chain; non-isothermal; plug flow; tanks-in-series

INTRODUCTION

Gas absorption process is widely used in industries for separating gases that are useful, toxic, or environmentally unfavorable species. As a consequence of the importance and being widespread of absorption operation, the subject has received wide consideration from the theoretical and experimental point of view (1,2). More recently, experimental attempts are made to improve the effectiveness of spray absorbers by applying the advantages of impinging streams. The coaxial impinging streams apparatus, which utilizes a unique type of flow behavior to intensify the transfer processes in heterogeneous systems, was first described by Elperin (3). Figure 1 shows schematically the impinging streams configuration. As can be seen, two streams flowing counter-currently on a same axis collide with each other at an impingement zone. Later, Tamir et al. (4) investigated the application of this configuration in a series of operations such as mixing of gases and solids, absorption, extraction, drying, and dissolution processes.

The transport processes are intensified in impinging streams absorbers due to the following effects:

- Increasing relative velocity between gas and drops and hence decreasing the fluid-side mass transfer resistance.
- Increasing the mean residence time of drops inside the impinging streams system due to their penetration into the opposed stream.

Investigations on impinging streams absorbers began in the mid-1980s and were mainly concentrated in Israel. Up to the 1990s all attempts made were essentially on the basis of fundamental aspects which focused mainly on analyzing and verifying the enhancement of transport phenomena due to the existing of impinging streams and also, searching for related experimental evidences (4). Sohrabi et al. (5) developed a stochastic model to predict the residence time distribution in two-impinging streams reactors. Also, a desulfurization absorber comprising of coaxial cylinders with impinging streams was developed, modeled, and tested with $Ca(OH)_2$ as the sorbent by Berman et al. (6). Furthermore, Wue et al. (7) investigated the flue gas desulfurization by absorption in an impinging streams gas–liquid reactor which was developed for systems involving fast reaction(s) in liquid phase.

In spite of the fact that the principles of impinging streams reactors have been developed for more than half a century, the performance analysis of such devices, especially absorbers, from the viewpoint of the mathematical modeling and simulation, has not been investigated widely up to now. In the present study, an attempt has been made to develop some mathematical models for predicting the rate of gas absorption in a coaxial impinging streams absorber with single phase nozzles, i.e., the gas and liquid were brought into contact only after leaving

Received 31 December 2009; accepted 5 May 2010.
Address correspondence to Amir Rahimi, Department of Chemical Engineering, College of Engineering, University of Isfahan, Isfahan, Iran. Tel.: + 98 311 7934039; Fax: +98 311 7934031. E-mail: rahimi@eng.ui.ac.ir

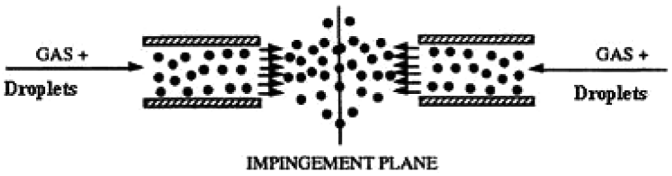

FIG. 1. Schematic diagram of a coaxial two impinging streams configuration.

the spray nozzle. In addition, based on the schematic diagram demonstrated in Fig. 2 the effectiveness of two-impinging streams absorber is investigated. Figure 2a is a schematic diagram of a coaxial two-impinging streams absorber which is compared with the conventional absorber (Fig. 2b). The latter is simply obtained by operating each half of Fig. 2a separately. If one notes the absorption rate of the absorbed gas in the two-impinging streams absorber by R_2 (Fig. 2a), and that of a single stream absorber by R_1 (Fig. 2b), the enhancement factor parameter may be defined as follows (8):

$$E_h = \frac{R_2}{2R_1} \succ 1 \qquad (1)$$

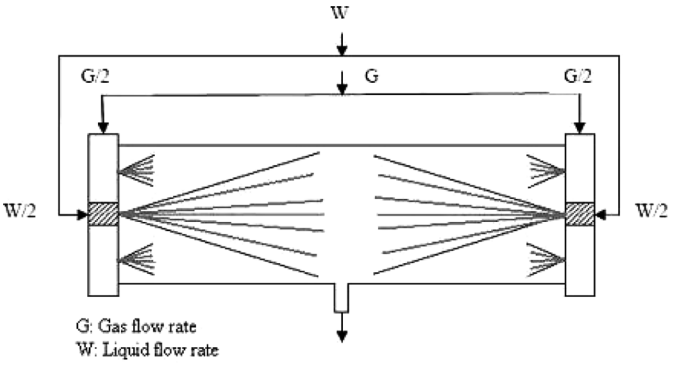

(a) **Two impinging streams absorber**

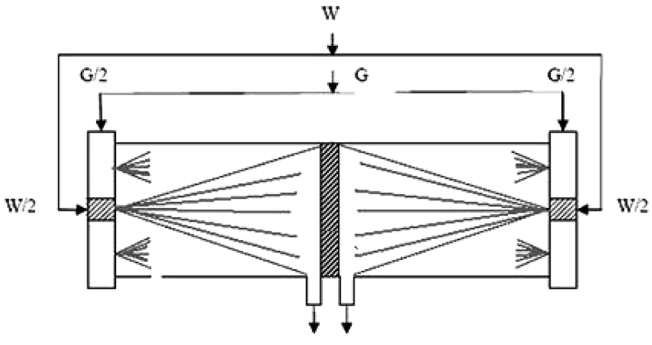

(b) **Two single-streams absorbers**

FIG. 2. Schematic diagrams of (a) two-impinging streams; and (b) two single-stream absorbers.

The two-impinging streams configuration is more efficient than the single one simply if E is greater than unit.

MATHEMATICAL MODELS

In this section, the actual behavior of a coaxial two impinging streams absorber (TISA) is modeled based on the concept of plug flow and ideal stirred tank systems. For this purpose, using the conservation laws of mass, energy, and momentum, the governing equations are derived for three different models including: the plug flow model, the tanks-in-series model, and a proposed model on the basis of Markov-Chain analysis. The main assumptions considered for the absorption process are listed below:

- The re-atomization and coalescence of drops are neglected.
- The thermo-physical properties of the gas are kept constant through the gas–liquid contact time apart from their variation with temperature.
- There is no heat exchange between the system and the surrounding.
- The drops are considered as a lumped system.
- The low solubility of gases in the solvents such as CO_2-water is determined by the Henry's law.

It should be noted that the effect of liquid vaporization is considered in each model due to high heat and mass rates. Also, in order to approach a realistic model, the distribution of the liquid droplets also is implemented in the models.

Plug Flow Model

In this case the TISA is a reactor whose velocity profile is rather simple and describable by some mathematical expression. The flow of each phase is considered as plug flow, so the distribution of temperature, velocity, and concentration in radial direction are neglected.

Tanks-in-Series Model

The tanks-in-series model is simple, it can be used with any kinetics, and it can also be extended without too much difficulty to any arrangement of compartments, with or without recycle. In this model, the drops flow through a series of M ideal, equal-sized stirred tanks, as shown in Fig. 3. Therefore, the turbulency of the impingement zone is simply possible to be modeled.

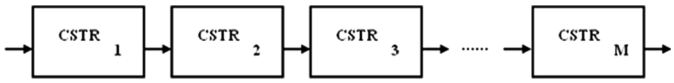

FIG. 3. Schematic diagram of TISA replaced with M stirred tanks in series.

In relation to M equal-sized stirred tanks arranged in series, the residence time distribution function (E) and the theoretical variance (σ^2_{Model}) are given by (9):

$$\bar{t}_{\text{model}}E = \left(\frac{t}{\bar{t}_{\text{model}}}\right)^{M-1}\frac{M^M}{(M-1)!}e^{-tM/\bar{t}_{\text{model}}} \tag{2}$$

$$\sigma^2_{\text{model}}(t) = \frac{\bar{t}^2_{\text{model}}}{M} \tag{3}$$

M and $\bar{t}_{model}$ are the two parameters of this model that should be determined on the basis of experimental RTD data by the following conditions:

$$\sigma^2_{\text{exp}} = \sigma^2_{\text{model}}; \qquad \bar{t}_{\text{exp}} = \bar{t}_{\text{model}} \tag{4}$$

where

$$\sigma^2_{\text{exp}}(t) = \frac{\int_0^\infty (t-\bar{t}_{\text{exp}})^2 C dt}{\int_0^\infty C dt} \tag{5}$$

$$\bar{t}_{\text{exp}} = \frac{\int_0^\infty tC dt}{\int_0^\infty C dt} \tag{6}$$

In Fig. 4, the experimental RTD data presented for a coaxial TISA in the literature (5) is compared with the theoretical results obtained from the tanks-in-series model. As observed, M varies between 2 and 3 for the desired coaxial TISA depends on operational conditions. In this study we consider three tanks in series.

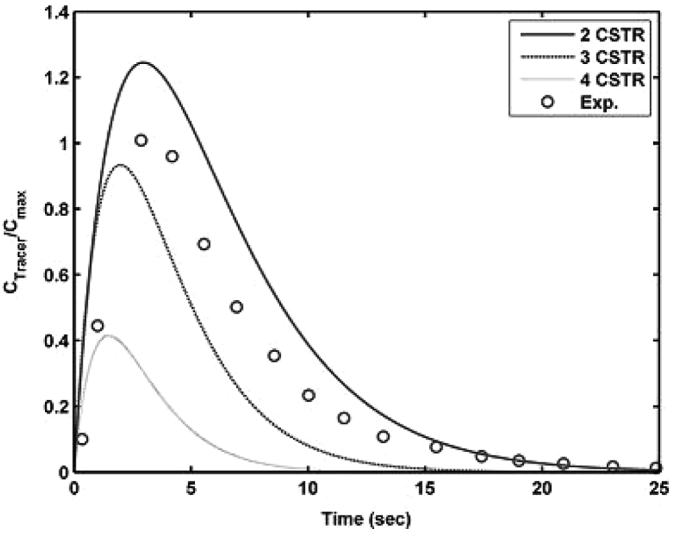

FIG. 4. Comparison of theoretical RTD curve obtained by tanks-in series model with experimental RTD data (5).

Markov-Chain Model

A Markov process is a mathematical probabilistic model that is very useful in the study of complex systems (4). In this model, if the initial state of a system and the probabilities to move forward to other states are known, it is possible to predict the next state of the system. In other words, past history is immaterial for predicting the future; this is the key element in the Markov chains analysis.

Using the information contained in the transition probability matrix P and the probability vector of the previous step $S(m)$, the state probability vector after m transitions, $S(m+1)$, is determined by the following formula (4,9):

$$S(m+1) = S(m)\cdot P \tag{7}$$

On the other hand, the probability that a system will be in state j after $m+1$ transition is given by (4,9):

$$s_j(m+1) = \sum_{i=1}^{N} s_i(m)p_{ij} \qquad m = 1,2,3,\ldots \tag{8}$$

where $s_i(m)$ is the ith element of the state probability vector $S(m)$, and p_{ij} is i, jth element of the transition probability matrix P (9). In addition, the following conditions hold:

$$\sum_{i=1}^{N} s_i(m) = 1; \qquad \sum_{j=1}^{N} p_{ij} = 1 \tag{9}$$

The characteristic of the Markov model is to predict the behavior and the response of a complicated system with respect to the residence time of fluid elements flowing through it. Also, this model, which consists of a series of perfectly mixed tanks, plug-flow systems, dead fluid elements, recycle streams, by pass and cross flow etc., has been applied to describe the non-ideal flow behavior of complex systems (9,10,11).

If N is the total number of states in the Markov model, $s_{N\text{-}1}(m)$ represents the impulse response of the system after m intervals of time length. Thus, the theoretical RTD of the system is obtained:

$$E(t) = RTD = \frac{s_{N-1}(t)}{\int_0^\infty s_{N-1}(t)dt} \tag{10}$$

For application of this expression, the two dimensionless parameters of the model, R and $\Delta\theta$, must be fitted by experimental RTD data. Figure 5 shows the alternative arrangement of vessels in the Markov process used in this study. It should be noted that R is the liquid recycle rate ratio ($r/\dot{m}_D$) and $\Delta\theta$ is the dimensionless time interval

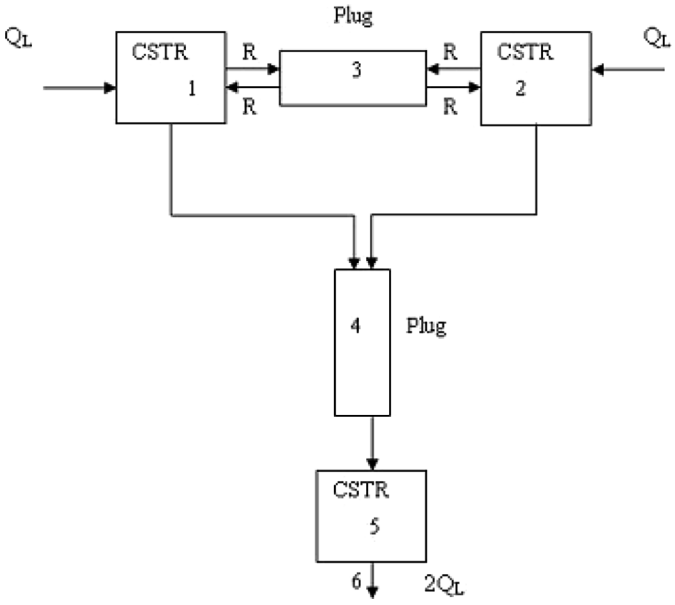

FIG. 5. Schematic diagram of vessels and flows in the Markov chain model.

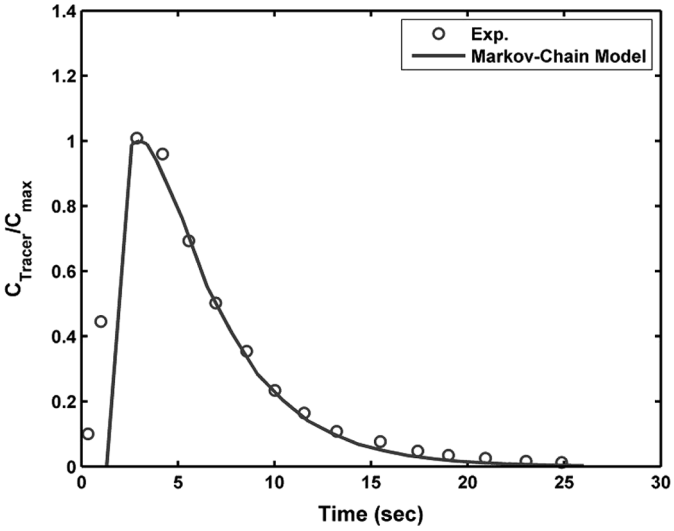

FIG. 6. Comparison of theoretical RTD curve obtained by Markov model with experimental RTD data (5).

defined as the ratio of the minimum residence time of the liquid drops in a Markov vessel to the mean residence time of the liquid drops in the TISA ($\bar{t}_j/\bar{t}$).

The transition probability matrix and the initial state probability vector for this alternative arrangement are as the below, respectively:

$$P = \begin{bmatrix} e^{-0.5n_v\Delta\theta} & 0 & \frac{R}{R+1}(1-e^{-0.5n_v\Delta\theta}) & \frac{1}{R+1}(1-e^{-0.5n_v\Delta\theta}) & 0 & 0 \\ 0 & e^{-0.5n_v\Delta\theta} & \frac{R}{R+1}(1-e^{-0.5n_v\Delta\theta}) & \frac{1}{R+1}(1-e^{-0.5n_v\Delta\theta}) & 0 & 0 \\ 0.5 & 0.5 & 0 & 0 & 0 & 0 \\ 0 & 0 & 0 & 0 & 1 & 0 \\ 0 & 0 & 0 & 0 & e^{-n_v\Delta\theta} & 1-e^{-n_v\Delta\theta} \\ 0 & 0 & 0 & 0 & 0 & 1 \end{bmatrix} \tag{11}$$

$$S(0) = [0.5 \quad 0.5 \quad 0 \quad 0 \quad 0 \quad 0] \tag{12}$$

Figure 6 shows a comparison of the theoretical RTD curve obtained by the Markov model with experimental RTD data (5). As previously mentioned, using the fitting technique and using the existing experimental RTD data (5) the point that the best adjustment is reached as $R = 0.95$ and $\Delta\theta = 0.037$.

GOVERNING EQUATIONS

The governing equations required for the above-mentioned models are presented below.

Mass Balance for Absorbed Gas in Gas Phase

The variation equation of mole fraction of the absorbed gas in the gaseous phase in a plug flow absorber may be derived as follows:

$$\frac{dy_A}{dz} = -\sum_{i=1}^{N} \frac{A_{Di} \cdot N_{Ai}}{G \cdot V_{Di}} \left[1 + \frac{N_{Bi}}{N_{Ai}} y_A\right] \tag{13}$$

For an ideal stirred tank it yields:

$$(G \cdot y_A)|_{\text{in}} - (G \cdot y_A)|_{out} - \sum_{i=1}^{N} N_{Ai} \cdot A_{Di} \cdot \bar{t}_j = 0 \tag{14}$$

In the above equations, A_{Di} is the interfacial area of ith class of drops diameter ($A_{Di} = 6Q_L \cdot P_i/D_{Di}$), where P_i is the volume percent of ith class of drops diameter and can be calculated by:

$$P_i = f(D)dD. \tag{15}$$

Which f (D) is the frequency volume distribution function of drops.

The flux of absorption (N_{Ai}) and the flux of solvent vaporization (N_{Bi}) can be calculated by the following relations, respectively:

$$N_{Ai} = k_{yAi}(y_A - y_A^*) \tag{16}$$

$$N_{Bi} = k_{yi}(y_B^* - y_B) \tag{17}$$

In the above equations, y_A^* is the equilibrium mole fraction of the absorbed gas on the drop surface. Also y_B^* is equilibrium mole fraction of gas humidity which can be calculated by using the Antoine equation.

In Eqs. (13) and (14), parameters such as absorption flux, flux of solvent vaporization, gas humidity, mole fraction of the absorbed species in the liquid, drop diameter, drop velocity, gas, and drop temperature have implicit and explicit effects on the mole fraction of the absorbed gas through the absorber length.

Energy Balance for the Gaseous Phase

In the impinging streams absorber, gas temperature changes due to the convective heat transfer by the drops. Also, a part of gas energy is consumed for raising the vapor temperature from the drop surface temperature to the gas temperature. The energy balance equation for the gaseous phase in a plug flow impinging streams system will give us:

$$\frac{dT_g}{dz} = -\sum_{i=1}^{N} \frac{h_{Di} \cdot A_{Di}}{G'_y \cdot C_g \cdot V_{Di}}(T_g - T_{Di}) \tag{18}$$

In the case of an ideal stirred tank it yields:

$$G'_y(C_S(T_g - T_0))|_{\text{in}} - G'_y(C_S(T_g - T_0))|_{out} - \sum_{i=1}^{N} h_{Di} \cdot A_{Di} \cdot \bar{t}_j(T_g - T_{Di})|_{out} = 0 \tag{19}$$

Energy Balance Equation for Liquid Drop

The liquid injected drops by the nozzles at the entrance of a system may have a different temperature from the wet-bulb temperature of the entering gas (in the adiabatic spray systems). However, it may be assumed that the drop temperature reaches rapidly to the wet-bulb temperature of entering gas. In this study, using the energy balance equation for drops, the variation equation of drop temperature is obtained. This equation may be applied as a good checkpoint for model verification, since it is expected to predict a sharp temperature rise for drops followed by a constant value for other remaining lengths of the absorber (the wet-bulb temperature) (12). The equation for drop temperature variation in the case of a plug flow system may be obtained as follows:

$$\frac{dT_{Di}}{dz} = \frac{[h_{Di} \cdot \pi D_{Di}^2 \cdot (T_g - T_{Di}) - N_{Bi} \cdot \pi D_{Di}^2 \cdot M_B \cdot \lambda_0]}{m_{Di} \cdot C_{PL} \cdot V_{Di}} \tag{20}$$

For an ideal stirred tank it may be given by:

$$\dot{m}_{Di} \cdot C_{PD}(T_{Di} - T_0)|_{\text{in}} - \dot{m}_{Di} \cdot C_{PD}(T_{Di} - T_0)|_{out} + h_{Di} \cdot A_{Di} \cdot \bar{t}_j(T_g - T_{Di})|_{out} - N_{Bi} \cdot M_B \cdot A_{Di} \cdot \bar{t}_j \cdot \lambda_0|_{out} = 0 \tag{21}$$

Mass Balance for Gas Humidity

The variation equation of the gas humidity due to the vaporization is obtained as the below.

For plug flow system:

$$\frac{dHu}{dz} = \sum_{i=1}^{N} \frac{N_{Bi} \cdot M_B \cdot A_{Di}}{G'_y \cdot V_{Di}} \tag{22}$$

For an ideal stirred tank:

$$G'_y Hu|_{\text{in}} - G'_y Hu|_{out} + \sum_{i=1}^{N} N_{Bi} \cdot M_B \cdot A_{Di} \cdot \bar{t}_j|_{out} = 0 \tag{23}$$

Mass Balance for Liquid Drop

The variation equation of the drop diameter in any location of the system is obtained by taking the mass transfer rate of evaporation into account, as follows:

For a plug flow system:

$$\frac{dD_{Di}}{dz} = -\frac{2N_{Bi} \cdot M_B}{\rho_L \cdot V_{Di}} \tag{24}$$

For an ideal stirred tank:

$$D_{Di}^3|_{\text{in}} - D_{Di}^3|_{out} - \frac{6N_{Bi} \cdot M_B \cdot \bar{t}_j}{\rho_D} D_{Di}^2|_{out} = 0 \tag{25}$$

Mass Balance for Absorbed Gas Species in a Liquid Drop

If x_A defined as the molar ratio of the absorbed gas species to the drop. The variation equation of x_A is obtained as follows:

For a plug flow system:

$$\frac{dx_A}{dz} = \frac{N_{Ai} \cdot \pi D_{Di}^2}{m_{Di} \cdot V_{Di}} \tag{26}$$

For ideal stirred tank:

$$(\dot{m}_{Di} x_A)|_{out} - (\dot{m}_{Di} x_A)|_{\text{in}} - N_{Ai} \cdot A_{Di} \cdot \bar{t}_j = 0 \tag{27}$$

Momentum Balance for a Liquid Drop

The variation equation of drop velocity in a plug flow system is obtained by the use of Newton's second law of motion, as follows:

$$m_{Di}\frac{d\vec{V}_{Di}}{dt} = m_{Di}\vec{a} - \left(\frac{m_{Di}}{\rho_{Di}}\right)\rho_g\vec{a} \\ -0.5C_f\rho_g A_D|\vec{V}_{Di} - \vec{V}_g|(\vec{V}_{Di} - \vec{V}_g) \quad (28)$$

Where, C_F is the drag coefficient which is determined from the correlations proposed by Tamir (4). Substitution in Eq. (28) for the mass of the drop $m_{Di} = (\pi/6)\ D_{Di}^3\rho_{Di}$, and for the projected area of a drop in a plane perpendicular to its motion $A_D = (\pi/4)\ D_{Di}^2$, gives the following equation (9):

$$\frac{dV_{Di}}{dz} = -\frac{0.75C_f\rho_g}{V_{Di}\cdot\rho_{Di}D_{Di}}|V_{Di} - V_g|(V_{Di} - V_g) \quad (29)$$

For the deceleration stage, V_a and V_{Di} are in the opposite directions. Thus, Eq. (29) will read:

$$\frac{dV_{Di}}{dz} = -\frac{0.75C_f\rho_g(V_g + V_{Di})^2}{V_{Di}\cdot\rho_{Di}D_{Di}} \quad (30)$$

and for the acceleration stage, V_a and V_{Di} are in the same directions. Thus, Eq. (29) will read:

$$\frac{dV_{Di}}{dz} = \frac{0.75C_f\rho_g(V_g - V_{Di})^2}{V_{Di}\cdot\rho_{Di}D_{Di}} \quad (31)$$

REQUIRED PARAMETERS

Size Distribution Consideration

For each nozzle at a given pressure and liquid flow rate there is a unique drop size distribution. This characteristic usually is shown with cumulative or frequency size distribution curves for each operational condition. In this investigation, the size distribution data and existing cumulative curve of back-flow nozzle are used. The frequency distribution of the drop size as a function of the drop diameter is obtained as follows (12):

$$f(D) = \frac{0.0877 + 0.11237D - 0.000226D^2}{1 - 0.0153D + 8.765\times10^{-5}D^2 - 1.1\times10^{-7}D^3} \quad (32)$$

Heat and Mass Transfer Coefficients

The following correlation is presented for calculations of heat transfer coefficient in impinging streams system ($Sh_{Di} = Nu_{Di}$) (4):

$$Nu_{Di} = 1.96\times10^{-4}\left(\frac{L}{D_{Nozzle}}\right)^{-2.405}\left(\frac{V_r}{L^3}\right)^{-0.821}Re_{Di}^{1.512} \quad (33)$$

Correlation for Recycle Ratio

The recycling ratio (R) may be described as the ratio between the drag forces acting on a drop in a certain recycling zone to the flux of momentum of the drops entering this zone. The latter may be any zone between the mixed vessels that were assumed in the various stochastic models. Kitron et al. (13) suggested a theoretical model to reveal dependence on R:

$$R = \text{constant}\left(\frac{W_D}{W_a}\right)^{-\frac{1}{3}} \quad (34)$$

It is observed that the ratio R decreases by increasing the ratio W_D/W_a. This behavior is explained as follows. Increasing the above ratio is due to an increase in W_D or a decrease in W_a. Collisions between drops are enhanced; i.e., the recycle is reduced. By decreasing the gas flow rate, the inertia of drops becomes lower, and so does their penetration and therefore R (4).

Heat and Mass Transfer Area

The actual area for the heat and mass transfer inside each vessel, namely, $A_{Di}\cdot\bar{t}_j$ must be determined based on RTD data and hold up of drops. However, if each of these requirements is not known, the area cannot be determined. For this purpose, Tamir (4) suggested the effective heat and mass transfer area (A_{eff}) as the basis of calculation, as follows:

$$A_{eff,D_i} = 6\frac{V_r}{D_{D_i}}\frac{W_a}{W_D}\frac{\rho_a}{\rho_D} \quad (35)$$

METHOD OF SOLUTION

All the above-mentioned equations are solved numerically using the fourth-order Runge-Kutta method for both the case of plug flow systems and ideal stirred tanks. In the case of stirred tanks model some trail and error methods are also utilized.

RESULTS AND DISCUSSION

Figure 7 shows the effect of both gas and liquid flow rates on the average absorption rate of CO_2 into water. The results are obtained from each of the three developed models and compared with the experimental data extracted from literatures (8,14). It should be noted that the temperature and pressure in experimental conditions varied in the range of 20–26°C and 730–740 mm Hg, respectively. The diameter of nozzles is 1.2×10^{-3} m. Also, the results of the models have been obtained for similar operating conditions.

As seen, increasing both the gas and liquid flow rates will increase the average absorption rate. When the gas

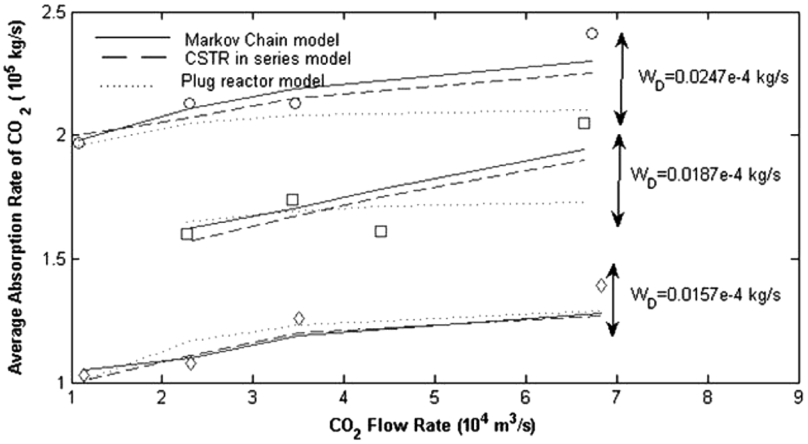

(a) CO_2-water system

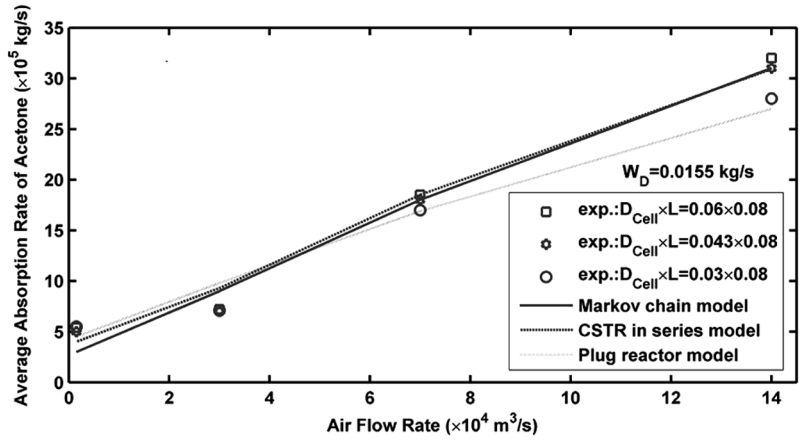

(b) Acetone-water system

FIG. 7. The effects of gas and liquid flow rates on the average absorption rate in TISA.

flow rate increases, the relative velocity and thus the gas-side mass transfer coefficient increases. However, as shown in Fig. 7a, the effect of the liquid flow rate is more significant than that of the gas flow rate. Increasing the liquid flow rate will increase the mass transfer area of the liquid drops. Since in the CO_2-water system the main mass transfer resistance lays in liquid side, increasing the mass transfer area increases the overall separation efficiency. The observed deviation between the model results and the experimental ones in higher values of both gas and liquid flow rates may be due to the re-atomization phenomenon which is ignored in the proposed models. The results of each model together with the deviations from the experimental data are presented in Table 1. As can be seen from Fig. 7 and Table 1, the predictions of the Markov chain model show a better agreement with the experimental data.

In Fig. 8, the results of models for average absorption rate are compared with the experimental data reported by Tamir and Herskowits (8) and Tamir (14). In this figure the effect of inlet nozzles' distance is investigated on the average absorption rate. A relatively good agreement can be observed between the model results and the experimental data. It is observed that an increase in gas flow rate causes the increase in the average rate of gas absorption since it reduces the gas-side mass transfer resistance. However, this impressibility is not sharp and big because as mentioned before the main mass transfer resistance is on the liquid side. On the other hand, the main mass transfer resistance of acetone-water system (Fig. 8b) is on the gas side; therefore, the characteristics of impinging streams may be successfully applied to this system. According to the experimental data in Fig. 8a, $L = 0.08$ may be considered as the optimal distance between nozzles (4), although the variation in the absorption rates against L, which is shown in Figs. 8a and 8b, is not significant. Notice that in Fig. 8a the closeness of the results of models makes us present the results of the plug flow model alone.

TABLE 1
The effects of gas and liquid flow rates on the average absorption rate in TISA for CO_2-water system

Q_{CO_2} ($\times 10^5$ m^3/s)	W_D ($\times 10^4$ kg/s)	$D_{Cell} \times L$	Rate of absorption (kg/s)				Relative error % $= \frac{\lvert Exp. - Model \rvert}{Exp.} \times 100$		
			Exp.	Plug reactor	CSTR in series model	Markov-Chain model	Plug reactor	CSTR in series model	Markov-Chain model
1.08	0.0246	0.03×0.1	1.97	1.96	2.01	1.98	0.51	2.03	0.51
2.30	0.0246	0.03×0.1	2.13	2.05	2.07	2.11	3.76	2.82	0.94
3.45	0.0246	0.03×0.1	2.13	2.08	2.15	2.19	2.35	0.94	2.82
6.72	0.0246	0.03×0.1	2.41	2.10	2.25	2.30	12.86	6.64	4.56
2.27	0.0187	0.03×0.1	1.60	1.65	1.57	1.62	3.12	1.88	1.25
3.43	0.0187	0.03×0.1	1.74	1.69	1.67	1.70	2.87	4.02	2.30
4.40	0.0187	0.03×0.1	1.61	1.71	1.75	1.78	6.21	8.70	10.56
6.64	0.0187	0.03×0.1	2.05	1.73	1.90	1.94	15.61	7.32	5.37
1.13	0.0157	0.03×0.1	1.03	1.01	1.01	1.05	1.94	1.94	1.94
2.31	0.0157	0.03×0.1	1.08	1.17	1.11	1.11	8.33	2.78	2.78
3.50	0.0157	0.03×0.1	1.26	1.23	1.21	1.19	2.38	3.97	5.56
6.82	0.0157	0.03×0.1	1.39	1.29	1.27	1.28	7.19	8.63	7.91
Max Relative Error %							15.61	8.70	10.56
Min Relative Error %							0.51	1.94	0.51
Average Relative Error %							5.59	4.31	3.87

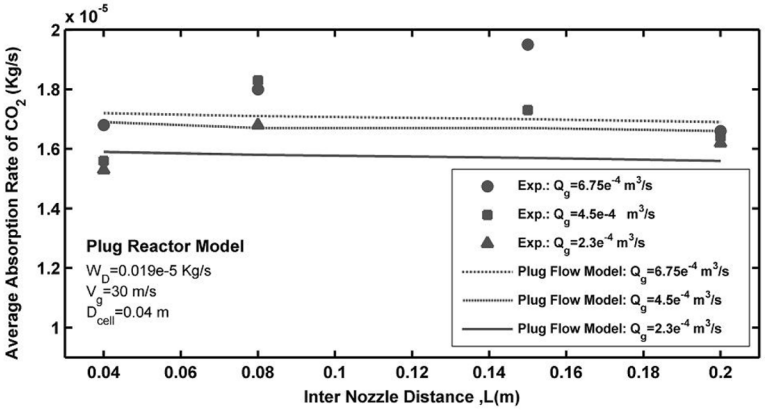

(a) CO_2-water system

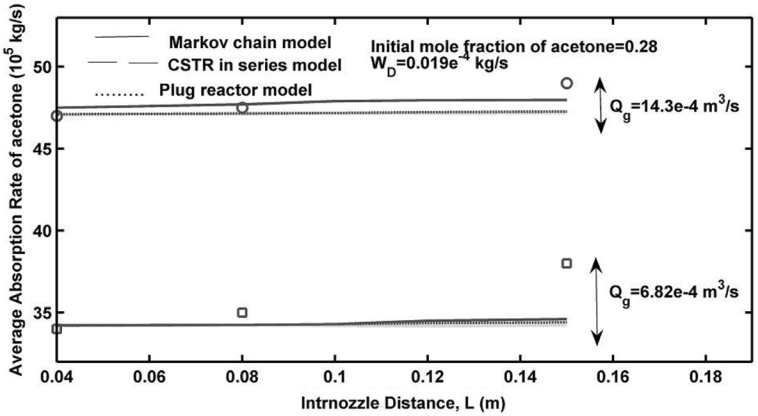

(b) Acetone-water system

FIG. 8. The effect of inlet nozzles distance on the average absorption rate in TISA.

TABLE 2
The effect of inter nozzle distance on the average absorption rate in TISA for CO_2-water system

			Rate of absorption (kg/s)				Relative error $\% = \frac{\lvert Exp.-Model \rvert}{Exp.} \times 100$		
Q_{CO_2} ($\times 10^5\ m^3/s$)	W_D ($\times 10^4$ kg/s)	$D_{Cell} \times L$	Exp.	Plug flow model	CSTR in series model	Markov-Chain model	Plug flow model	CSTR in series model	Markov-Chain model
6.75	0.019	0.04×0.04	1.68	1.96	1.65	1.66	16.67	1.66	1.10
6.75	0.019	0.04×0.08	1.80	2.05	1.65	1.66	13.89	8.19	7.69
6.75	0.019	0.04×0.15	1.95	2.08	1.65	1.66	6.67	15.23	14.79
6.75	0.019	0.04×0.20	1.66	2.10	1.65	1.67	26.51	0.41	0.76
4.5	0.019	0.04×0.04	1.56	1.65	1.65	1.66	5.77	5.84	6.50
4.5	0.019	0.04×0.08	1.83	1.69	1.65	1.66	7.65	9.76	9.20
4.5	0.019	0.04×0.15	1.73	1.71	1.65	1.66	1.16	4.53	3.95
4.5	0.019	0.04×0.20	1.64	1.73	1.65	1.66	5.49	0.71	1.33
2.3	0.019	0.04×0.04	1.53	1.01	1.65	1.66	33.99	7.87	8.59
2.3	0.019	0.04×0.08	1.68	1.17	1.65	1.66	30.36	1.76	1.08
2.3	0.019	0.04×0.15	1.45	1.23	1.65	1.66	15.17	13.82	14.64
2.3	0.019	0.04×0.20	1.62	1.29	1.65	1.66	20.37	1.89	2.62
		Max Relative Error %					33.99	15.23	14.79
		Min Relative Error %					1.16	0.41	0.76
		Average Relative Error %					15.30	5.97	6.03

The results and errors of each model are presented in Table 2.

The effect of both the gas and liquid flow rates on the average absorption rate in a single stream absorber is investigated by the plug flow model and the results are shown in Fig. 9. The model results are compared with the experimental data reported by Tamir and Herskowits (8) which shows a relatively good agreement. As observed, with increasing the water flow rate, the average rate of absorption increases, which is explained as the results of increasing the number of drops and hence, the absorbing area. Also, an increase in the gas flow rate shows a negligible effect on the average rate of absorption in a CO_2-water system. According to the experimental data, an increase in the absorption-cell diameter yields a slight increase in the rate of absorption due to a reduction of the influence of the absorption cell wall (8).

Figure 10 depicts the variation enhancement factor, defined by Eq. (1), with the gas flow rate. As observed, both the gas and liquid flow rates have a negligible effect on the enhancement factor. According to the experimental data, the maximum amount of the enhancement factor is about 1.65, namely a 65% increase in absorption rate of CO_2 in TISA, in comparison with the single stream

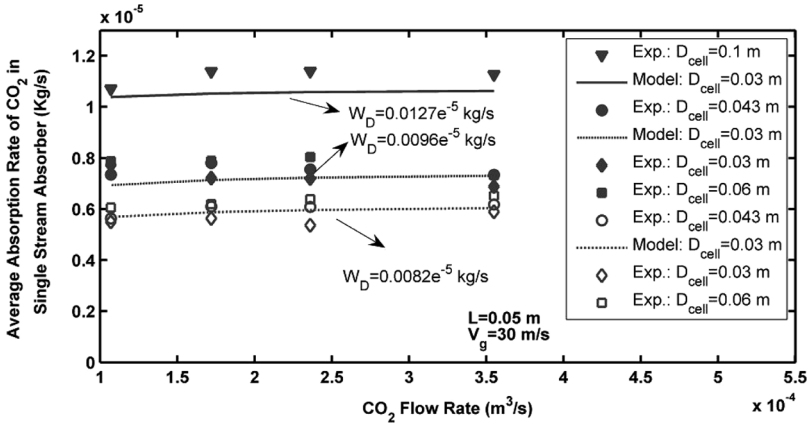

FIG. 9. Effects of gas and liquid flow rates on the average absorption rate of CO_2 in a single stream absorber.

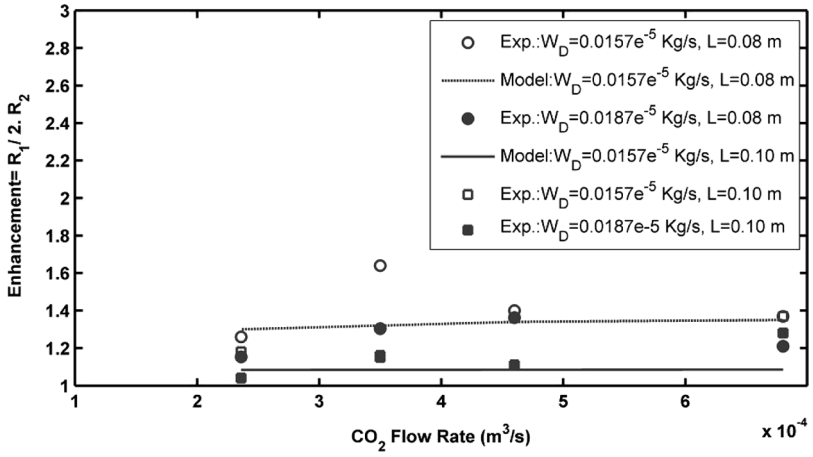

FIG. 10. Effects of gas and liquid flow rates on the enhancement factor.

absorber. It is concluded that the mass transfer in the presence of impinging streams is much higher than that of in the single stream absorber (in the absence of impinging streams). The main reasons may be summarized as follows:

- A sudden increase in the mass transfer coefficient in the impingement zone due to high relative velocity of the two phases.
- Increasing the mean residence time of drops due to performing oscillatory motions.

The results of the experiments on the absorption of CO_2 and acetone (8,14) into water indicate that the absorption rate in the absorber without partition shown in Fig. 2a is higher than that in the absorber with a partition shown in Fig. 2b, and the enhancing effect of impinging streams, too. In other words, the basic standard which was used for comparison is unreasonable. In the absorber with a medium partition, the flow configuration becomes two jets impinging fixed wall surfaces separately, and the latter enhances the transfer significantly (4), too. In other words, the intrinsic enhancing effect of impinging streams may be stronger than what is reported. For example, the impinging jet on a fixed wall may enhance the absorption rate by x times than normal, and impinging streams enhance by y times than the impinging jet on a fixed wall; so the total number of the times enhanced intrinsically by impinging streams than the normal should be $x \times y$.

The behavior of drop motion along the time and length of the TISA is shown in Fig. 11. In this figure $z = 0$ denotes the impingement plane. The drop has acceleration and

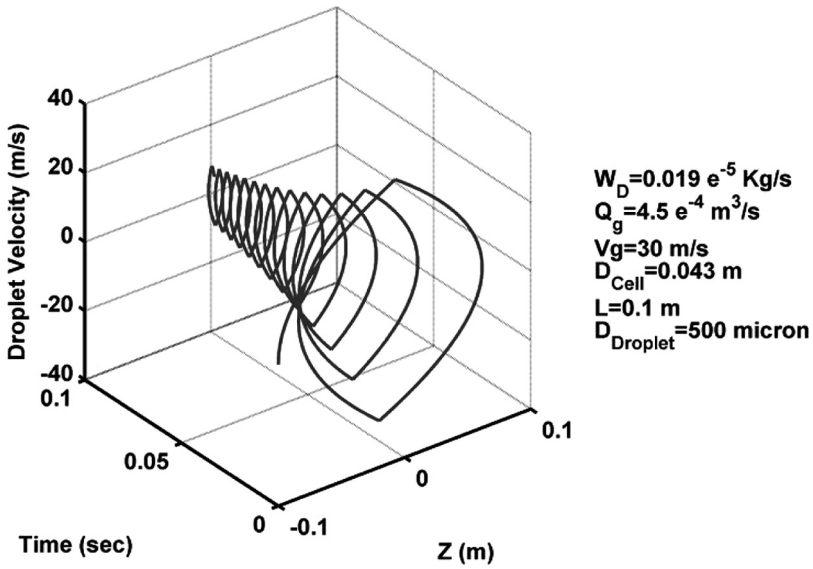

FIG. 11. Variation of drop velocity through time and length of TISA.

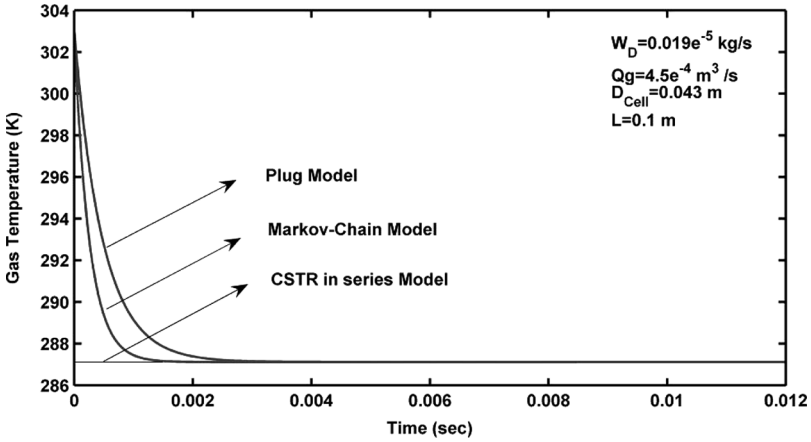

FIG. 12. Variation of gas temperature with time.

deceleration stages in the system depending on its inertia and also the drag force of the gas phase. After performing several oscillatory motions, the drop exists in the system. As can be seen, the maximum velocity and the penetration distance of drop in the impinging zone are reduced continuously as time progresses.

The variation of gas temperature through the contact time of the two phases is determined by the three models and is shown in Fig. 12. The gas temperature decreases rapidly and reaches a constant value in a short time ($t = 0.0018$ s for the plug flow model). The increase of heat transfer coefficient due to the increase of relative velocity at the impinging zone promotes the convective heat transfer within two phases and causes to get a constant value in this duration.

The variation of gas humidity vs. time is demonstrated in Fig. 13 for the three prescribed models. The sudden vaporization of water drops and the increase of heat transfer coefficient due to increase of relative velocity of the two phases in the impingement zone cause a rapid increase in the gas humidity and then attains a constant and maximum value (the saturated humidity).

Figure 14 shows the temperature variation of drop with various initial drop diameters resulted from the plug flow model. The drop temperature decreases initially due to the sudden vaporization which follows by a rapid increase as the result of increasing heat transfer coefficient in the impingement zone. The drop reaches its maximum and constant value (the wet-bulb temperature of entering gas) in the impingement zone. According to the constant temperature of drop, hereafter only, heat transfer causes the evaporation of the drop surface. As can be seen, by increasing the drop diameter, the variation rate of the drop temperature decreases. It should be noted that the variation of drop temperature is insignificant due to the high values of liquid to gas ratios used in such a system.

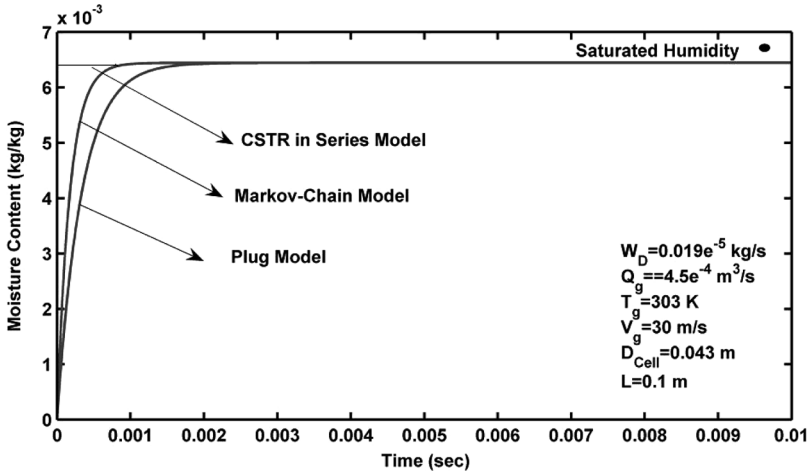

FIG. 13. Variation of gas humidity with time.

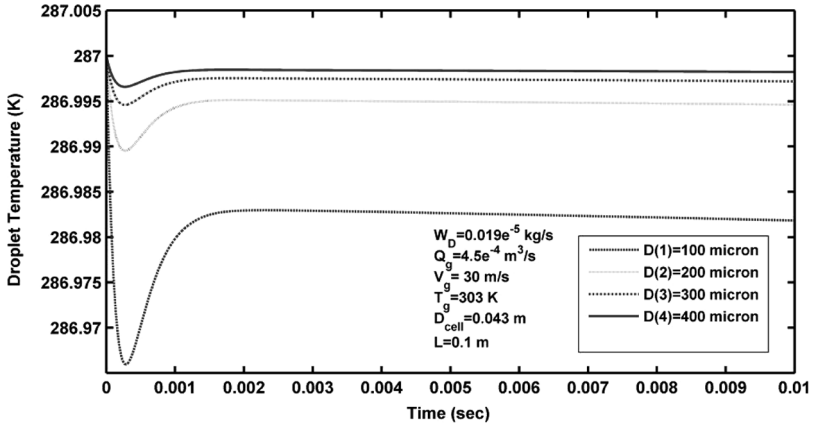

FIG. 14. Variation of drop temperature with time.

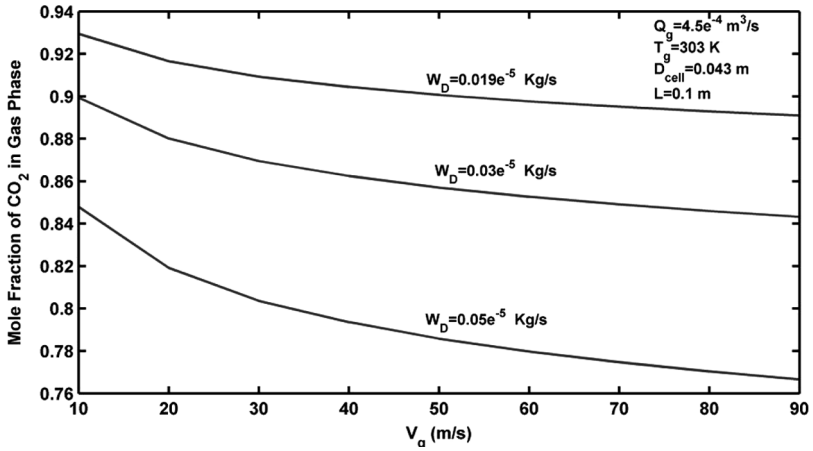

FIG. 15. Effect of gas velocity on the final mole fraction of CO_2 in the gas phase.

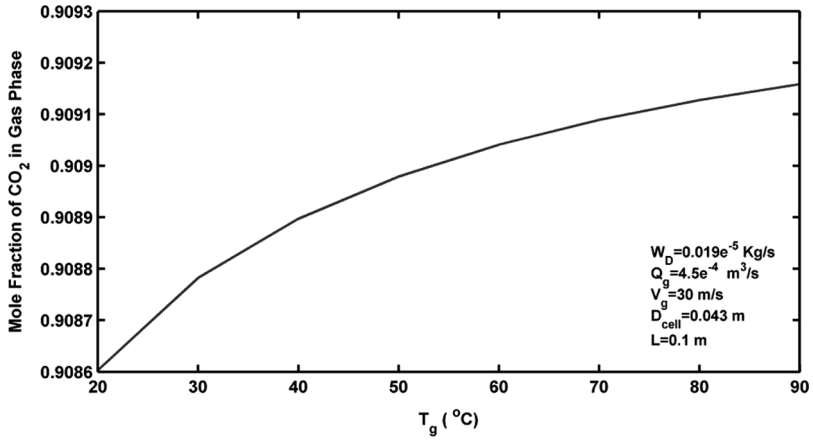

FIG. 16. Effect of gas temperature on the final mole fraction of CO_2 in the gas phase.

The effect of gas velocity on the final mole fraction of CO_2 in various liquid flow rates is shown in Fig. 15. It is assumed that residence time distribution of drops inside the system is the same and the gas velocity does not affect it. The increase of gas velocity causes the increase in the absorption rate of CO_2 and consequently, the decrease of the final mole fraction of CO_2 in the gas phase due to the increase of relative velocity and turbulency of the system. Furthermore, it is clearly demonstrated that increasing the liquid flow rate increases the absorption rate of CO_2 and consequently, decreases the final mole fraction of CO_2 in the gas phase due to the increase in the number of drops and hence the absorbing area.

Figure 16 shows the effect of gas temperature on the final mole fraction of CO_2 in the gas phase. As can be seen, the final mole fraction of CO_2 in the gas phase increases slightly by the increase in gas temperature, as a result of decreasing the physical absorption rate.

CONCLUSIONS

Three different mathematical models are presented and examined to predict the performance of two-impinging streams absorbers. By the comparison of the model results with the corresponding experimental data extracted from literatures (8,14), the preciseness of the suggested models is considered to be satisfactory, while the model based on the Markov-Chain analysis shows a better agreement in the presence of RTD data. The predictions of this model is within ±6% (average relative error) making it a valuable approach to design a large-scale absorber. In addition, the following major conclusions are obtained.

- Increasing the inlet nozzle distance offers a negligible effect on the absorption rate due to the contrast of increasing the residence time and decreasing the turbulency.
- The influence of liquid flow rate on the absorption rate is much higher than other operational parameters.
- The enhancing effects of impinging streams related to single stream absorbers was verified. Thus, TISA is considered to be more suitable and effective for carrying out the absorption process in comparison with the conventional systems.

NOMENCLATURE AND UNITS

a	External acceleration, $m^2 s^{-1}$
A_D	Projected area of a drop, m^2
A_{eff}	Effective Area, m^2
C_f	Drag coefficient
C_P	Heat capacity, $j kg^{-1} K^{-1}$
D_{AL}	Diffusivity of species A in solvent, $m^2 s^{-1}$
D_{BL}	Diffusivity of species B in solvent, $m^2 s^{-1}$
d	Diameter of spray nozzle, m
E_h	Enhancement factor, dimensionless
$f(D)$	Frequency distribution of drop, dimensionless
G	Gas flow rate, $kmole s^{-1}$
G_y	Gas flow rate (dry basis), $kg s^{-1}$
h	Heat transfer coefficient, $Wm^{-2} K^{-1}$
Hu	Gas humidity, kg water kg dry gas^{-1}
K	Mass transfer coefficient, $m^2 s^{-1}$
k_{yA}	Mass transfer coefficient for species *A* in gas film, $kmole m^{-2} s^{-1}$
k_{yB}	Mass transfer coefficient for species B in gas film, $m s^{-1}$
L	Internozzle distance, m
m	Mass, kg
M	Molecular weight, $kg kgmol^{-1}$
N_A	Flux of absorption, $kmole m^{-2} s^{-1}$
N_B	Flux of vaporization, $kmole m^{-2} s^{-1}$
Q_L	Liquid flow rate, $m^3 s^{-1}$
R	Recycling ratio, dimensionless
t	Time, s
T	Temperature, K
V	Velocity, $m s^{-1}$
V_r	Volume of absorber, m^3
y_A	Mole fraction of absorbed gas
y_B	Mole fraction of solvent

Greek Letters

ρ	Density, $kg m^{-3}$
λ_0	Heat of vaporization, $j kg^{-1}$
μ	Viscosity, $N s m^{-2}$
ν	Kinematic viscosity, $m^2 s^{-1}$

Dimensionless Groups

Ha	Hatta Number
Pr	Prandtl Number
Re	Reynolds Number
Sc	Schmidt Number
Sh	Sherwood Number

Subscripts

A, B	Absorbed gas and solvent components, respectively
D	Drop
exp	Experimental values
L	Liquid
g	Gas
i	Drop size identification
ii	Initial property of *i*th size of drops
D_i	Diameter of *i*th size of drops
model	Theoretical or model results

Superscripts

*	Equilibrium

REFERENCES

1. Charpentier, J.C. (1981) Mass transfer rates in gas-liquid absorbers and reactors. *Adv. Chem. Engng.*, 11: 1–133.
2. Charpentier, J.C. (1982) What's new in absorption with chemical reaction. *Trans. Instn Chem. Engrs.*, 60: 131–156.
3. Elperin, I.T. (1961) Heat and mass transfer in opposing currents. *Journal of Engineering Physics*, 6: 62–68.
4. Tamir, A. (1994) *Impinging-Stream Reactors: Fundamental and Applications*; Elsevier: Amsterdam.
5. Sohrabi, M.; Jamshidi, A.M. (1997) Studies on the behaviour and application of the continuous two impinging streams reactors in gas-liquid Reactions. *Journal of Chemical Technology Biotechnol.*, 69: 415–420.
6. Berman, Y.; Tanklevsky, A.; Oren, Y.; Tamir, A. (2000) Modeling and experimental studies of SO_2 absorption in coaxial cylinders with impinging streams: Part 1. *Chemical Engineering Science*, 55: 1009–1021.
7. Wu, Y.; Lib, Q.; Lia, F. (2007) Desulfurization in the gas-continuous impinging stream gas–liquid reactor. *Chemical Engineering Science*, 62: 1814–1824.
8. Tamir, A.; Herskowits, D. (1985) Absorption of CO_2 in a new two impinging stream absorber. *Chemical Engineering Science*, 40: 2149–2151.
9. Niksiar, A.; Rahimi, A. (2009) Application of Markov-chain analysis and Tanks-in-Series model in mathematical modeling of impinging stream dryers. *Drying Technology*, 27: 30–39.
10. Wen, C.Y.; Fan, L.T. (1975) *Models for Flow Systems and Chemical Reactors*; Marcel Dekker, Inc.: New York.
11. Petho, A.; Noble, R.D. (1982) *Residence Time Distribution Theory in Chemical Engineering*; Verlag Chemie.
12. Rahimi, A.; Taheri, M.; Fathikalajahi, J. (2002) Mathematical modeling of heat & mass transfer in hot gas spray system. *Chem. Eng. Comm.*, 189: 959–973.
13. Kitron, A.; Buchman, R.; Luzzatto, K.; Tamir, A. (1987) Drying and mixing of solids and particles RTD in four impinging streams and multistage two impinging streams reactors. *Industrial and Engineering Chemistry Research*, 26: 2454–2461.
14. Tamir, A. (1986) Absorption of acetone in a two impinging streams absorber. *Chemical Engineering Science*, 41: 3023–3030.